
FUSED DEEP CONVOLUTIONAL NEURAL NETWORK FOR PRECISION DIAGNOSIS OF COVID-19 USING CHEST X-RAY IMAGES

A PREPRINT

Hussin K. Ragb, Ian T. Dover

Department of Engineering
School of Electrical and Computer Engineering
Christian Brothers University
Memphis, Tennessee
{hragb, idover}@cbu.edu

Redha Ali

Department of Electrical and Computer Engineering
University of Dayton
300 College Park, Dayton, Ohio 45469
almahdir1@udayton.edu

September 21, 2020

ABSTRACT

With a Coronavirus disease (COVID-19) case count exceeding 10 million worldwide, there is an increased need for a diagnostic capability. The main variables in increasing diagnostic capability are reduced cost, turnaround or diagnosis time, and upfront equipment cost and accessibility. Two candidates for machine learning COVID-19 diagnosis are Computed Tomography (CT) scans and plain chest X-rays. While CT scans score higher in sensitivity, they have a higher cost, maintenance requirement, and turnaround time as compared to plain chest X-rays. The use of portable chest X-radiograph (CXR) is recommended by the American College of Radiology (ACR) since using CT places a massive burden on radiology services. Therefore, X-ray imagery paired with machine learning techniques is proposed a first-line triage tool for COVID-19 diagnostics. In this paper we propose a computer-aided diagnosis (CAD) to accurately classify chest X-ray scans of COVID-19 and normal subjects by fine-tuning several neural networks (ResNet18, ResNet50, DenseNet201) pre-trained on the ImageNet dataset. These neural networks are fused in a parallel architecture and the voting criteria are applied in the final classification decision between the candidate object classes where the output of each neural network is representing a single vote. Several experiments are conducted on the weakly labeled COVID-19-CT-CXR dataset consisting of 263 COVID-19 CXR images extracted from PubMed Central Open Access subsets combined with 25 normal classification CXR images. These experiments show an optimistic result and a capability of the proposed model to outperforming many state-of-the-art algorithms on several measures. Using k-fold cross-validation and a bagging classifier ensemble, we achieve an accuracy of 99.7% and a sensitivity of 100%.

Keywords coronavirus, chest X-ray radiograph, convolutional neural networks, deep transfer learning, ensemble neural networks, bagging ensemble, majority vote classifier

1 Introduction

In 2020, we have seen a daily rapid increase in the COVID-19 case count reported from 20,000 daily new cases in mid-March to nearly 140,000 new cases daily in late-June. It is imperative that fast and efficient methods of testing be adopted to meet the increased demand. LabCorp's COVID-19 at-home test kit, a test swab that is taken from home then delivered to a laboratory setting, is currently listed at over \$100 (USD) and has a multi-day turnaround time due to shipment and laboratory procedures. As a less expensive option, Quidel sells reverse transcriptase-polymerase chain reaction (RT-PCR) assays at around \$20 (USD) per test to health care providers for viral nucleic acid detection; however, while RT-PCR tests are considered the gold standard for COVID-19 diagnosis, they suffer from low sensitivity and a turnaround time in many cases exceeding 4 hours.

RT-PCR testing has been adopted as the forerunner in the Coronavirus pandemic, but these tests yield a sensitivity of 91% in practice [1]. CT images have been shown to have higher sensitivity in some cases to detect COVID-19 infections in patients with false-negative RT-PCR results with reported sensitivities as high as 97-98% [1]. Researchers from Wuhan, China developed a deep learning model named COVID-19 Detection Neural Network (COVNet) using chest CT images, dividing results into 3 class labels: COVID-19, community-acquired pneumonia (CAP), and non-pneumonia. This network acquired a sensitivity of 90% and specificity of 96% [2].

Nevertheless, while recent COVID-19 radiology literature has extensively explored the use of CT imagery, there are several benefits to applying CXR imagery to COVID-19 testing: CXR imagery is relatively inexpensive compared to alternatives, has a decreased risk of infection, and is less invasive. CXR equipment is more widely available, especially in developing nations, and the maintenance requirement of sanitization is less than that for CT equipment. While the baseline sensitivity for CXR is 69%, [3, 4, 5] CXR can play a primary role of the initial screening for COVID-19. In many cases, for patients with high CXR abnormalities, further CT testing may be redundant, thus reducing the burden on radiology services worldwide. In this way, it is suggested that both CXR and CT be used as a two-pronged approach to early COVID-19 detection whereas CXR can be used as a first-line triage tool.

From a pictorial perspective of radiological images, CXR is the less sensitive modality with ground glass densities (GGO) easily detectable on CT but not CXR; CXR densities often appear hazy while CT densities have a clear contrast. However, reticular opacities are often more apparent on CXR than on CT. On baseline CXR, consolidations are the most common finding, with COVID-19 and viral pneumonia producing lung opacities in multiple lobes as opposed to one in bacterial pneumonia which tends to be unilateral. COVID-19 pneumonia has prominent peripheral air space opacities which are readily identified by both CT and CXR with CT reporting peripheral lung distribution in 33-86% of cases [4, 5]. Diffuse air space diseases such as acute respiratory distress syndrome (ARDS) demonstrate similar patterns to CXR, but these COVID-19 lung opacities rapidly evolve into a diffuse coalescent or consolidative pattern with 1-3 weeks of symptom onset [6, 7]. One study reported that of 64 patients, consolidation was found in (30/64, 47%) of patients while GGO was found in (21/64, 33%). Common distribution locations included peripheral (26/64, 41%) and lower zone (32/64, 50%), with most showing bilateral involvement (32/64, 50%) [1]. Although very uncommon, pleural effusions were found in a small number of cases.

The structure of this study is inspired by [8]; Uses pre-trained variants of ResNet50, InceptionV3, and Inception-ResNetV2 to obtain prediction accuracies of 98%, 97%, and 87%, respectively [8]. This showed that ResNet50 is an effective pre-trained model for CXR COVID-19 detection. However, our study improved upon this previous work by expanding the dataset from 50 COVID-19 images [8] to 261 COVID-19 images from the COVID-19-CT-CXR [9] dataset and by introducing bagging ensembles to further increase accuracy. This manuscript is organized as follows: the dataset is covered in Section 2.1; data preprocessing is described in Section 2.2; Section 2.3 summarizes the network architectures used; deep transfer learning and ensemble learning are explained in Section 2.4 and 2.5, respectively; Section 2.6 and 2.7 outline the experimental setup and performance metrics, respectively. Section 3 contains the Discussion and obtained results for each neural network. Section 4 summarizes the work with a Conclusion.

2 Materials and Methods

2.1 Dataset

In this study, 261 COVID-19 chest X-ray images have been obtained from the open-source COVID-19-CT-CXR dataset [9]. These images were extracted from figures, associated captions, and subfigures in COVID-19 articles from the PubMed Central Open Access (PMC-OA) subset. Most figures found in the PMC-OA articles are compound figures, each consisting of several subfigures often being of multiple categories such as CT, CXR, or an assortment of 26 other scientific figures. A deep-learning model was designed to distinguish compound figures from other figure types [9]. The designed deep-learning model is a convolutional neural network pretrained on the ImageCLEF Medical dataset [10].

Many of the figures in the PMC-OA articles are not CT or CXR images. Therefore, a scientific figure classifier based on the DenseNet121 architecture was trained on 500 CXR images and 500 CT images taken from the NIH Chest X-ray and DeepLesion dataset, respectively. DenseNet121 was pretrained on the ImageNet dataset and fine-tuned with the last classification layer replaced with a fully connected layer using a softmax operation [9]. For text extraction, PMC-OA articles were downloaded through a RESTful web service. The articles were parsed for figure numbers and captions, and figure numbers and regular expressions were used to find where figures were cross-referenced [9].

2.2 Data Pre-processing

Images from the COVID-19-CT-CXR [9] dataset are taken at different centers, with different protocols, and with the potential for human error. To account for these differences and to artificially expand our limited dataset, we use random

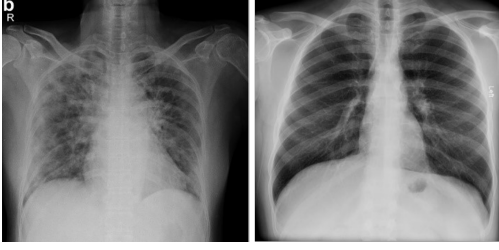


Figure 1: CXR Images of COVID-19 Cases

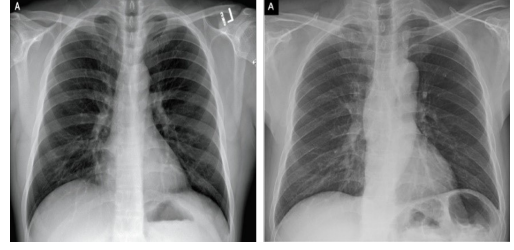


Figure 2: CXR Images of Normal Cases

x-axis and y-axis reflections each with a 50% probability, random rotation from 10 to -10 degrees, and a random x-axis and y-axis shear from -0.3 to 0.3 degrees.

Images from the COVID-19-CT-CXR dataset range in height from 224 to 2,703 pixels with an average of 387.5 pixels. Image width ranges from 224 to 1,961 pixels with an average of 472.4 pixels [9]. Each image is resized to fit the input of ResNet18, ResNet50, and DenseNet201 with an image input size of 224 x 224 pixels and the input of Xception with an image input size of 299 x 299 pixels.

2.3 Network Models

Three models – ResNet18 [11], ResNet50 [11], and DenseNet201 [12] – are pretrained on the ImageNet dataset then fine-tuned on the COVID-19-CT-CXR dataset with the final-layers replaced. Once fine-tuned, experiments are done to determine the robustness of individual ensemble network combinations.

2.3.1 ResNet

It has been shown that deep residual networks have increasing performance as layers are scaled up. However, these networks have a problem of diminished feature reuse known as the vanishing/exploding gradient problem [11, 13, 14]. To mitigate this problem, a new architecture called ResNet blocks was introduced to decrease depth and increase width of residual networks. ResNets use identity connections and stochastic depth to move signals from one layer to the next and to randomly drop layers to promote gradient flow, respectively. It is demonstrated that even shallow wide residual networks outperform other previous deep learning networks [11].

2.3.2 DenseNet

Research has shown that Dense Convolutional Networks (DenseNets) connecting each layer to every other layer in a densely connected block alleviate the vanishing/exploding gradient problem [12, 13, 14, 15], reduce parameter count, and encourage feature reuse. This means that for traditional convolutional networks with L connections between layers, a DenseNet will have $\frac{L(L+1)}{2}$ connections. Both ResNet and DenseNet share a similar characteristic in that they shorten the distance from earlier layers to later layers [12].

Network	Depth	Parameters (Millions)	Image Input Size
ResNet18	18	11.7	224 x 224
ResNet50	50	25.6	224 x 224
DenseNet201	201	20	224 x 224

Table 1: Network Models

2.4 Deep Transfer Learning

Data dependence, where deep learning has a huge dependence on large-scale datasets, is a serious problem. With an improvement in deep learning’s potential as a function of layer count, a linear relationship also exists between model scale and dataset size. Insufficient training data is eminent in bioinformatics datasets where data collection is an expensive and complicated process [16]. In the domain of bioinformatics, large-scale and well-annotated datasets are costly to produce, thus limiting the size of the dataset. Transfer learning allows for the use of datasets that are not identically distributed to the test dataset. Expounding further, an unrelated dataset can be used to train the early layers of a deep neural network responsible for the identification of edges, blobs, and colors. Then, the intended dataset – in this instance, COVID-19-CT-CXR – is used to train the neural network to identify complex features utilizing those earlier

edges, blobs, and colors [16]. A Survey on Deep Transfer Learning, Chuanqi Tan and colleagues characterize deep transfer learning into four distinct categories: instance-based, mapping-based, network-based, and adversarial-based [16]. For the purposes of this paper, network-based deep transfer learning is utilized. This involves the reuse of a partial-network (front-layers) pre-trained on a source domain then transferred to be retrained on the target domain. The front-layers are treated as a versatile feature extractor that is useful for other learning tasks. Studies the transition from generalized to specific features from the early-layers to the final-layers [17]. It is stated that first-layer features tend to learned features imitate the Gabor filters and color blobs [17]. is an in-depth study between network structure and transferability. It concludes that ResNet models are good candidates for deep transfer learning [16, 17]. The transfer learning models used in this paper were pre-trained on the ImageNet dataset used in the ImageNet Large-Scale Visual Recognition Challenge (ILSVRC) consisting of over a million images and a thousand class labels. For each network, the last three layers – fully connected, softmax, and classification layer – are replaced with the weights randomly initialized. The fully connected, softmax, and classification layers are responsible for identifying those features specific to COVID-19 detection.

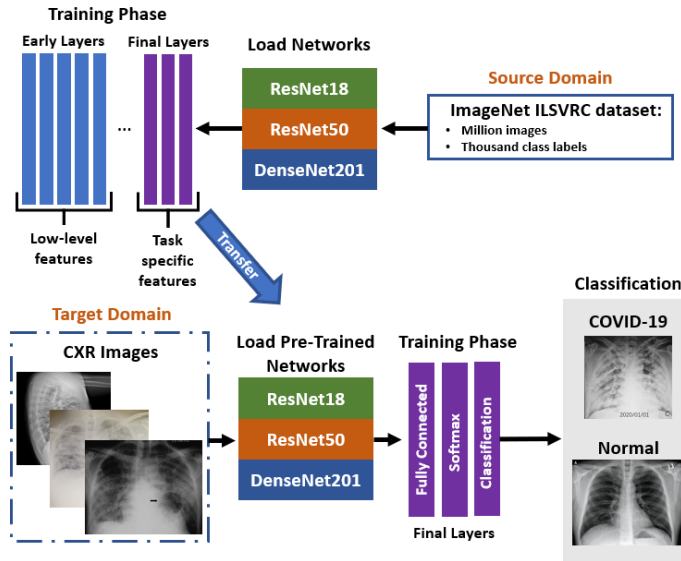


Figure 3: Network-Based Deep Transfer Learning for the Prediction of COVID-19 Patients Using CXR Images

2.5 Ensemble Learning

An ensemble is a set of classifiers whose predictions are combined. Research has shown that an ensemble tends to be more accurate than any individual classifier for various imaging applications [18, 8, 19]. Two popular methods of ensemble learning are bagging classifiers and boosting classifiers. Bagging classifiers train each classifier on varying subsets of the target dataset. This is particularly effective in “unstable” neural networks where small changes in the training set results in noticeable changes in test set predictions [20]. Moreover, each network in the ensemble may have an innate propensity to predict different subsets of the dataset more accurately, further supporting the bagging classifier’s effectiveness. As a result, bagging classifiers generally always outperform any individual classifier in the ensemble [20]. Boosting classifiers are a group of methods which involve altering the input dataset to the training phases of proceeding networks in an ensemble based on the performance of preceding networks. This is the practice of tailoring the input datasets of networks such that an optimal dataset representation is achieved that is non-reliant on input variance across the ensemble classifier. This ensemble method can vastly outperform bagging classifiers, but it has the potential to perform worse than an individual network in the classifier. Boosting classifier performance is heavily dependent on features of the target dataset [20]. For this experiment, the bagging approach is adopted to maximize performance. Each network is trained using k-fold cross-validation. The mean accuracy is measured across each fold of the trained models as seen in Figure 5. The output classification of the three selected networks are then grouped into a majority vote classifier ensemble neural network. A majority vote classifier takes the mode of the binary classifications as seen in Figure 4.

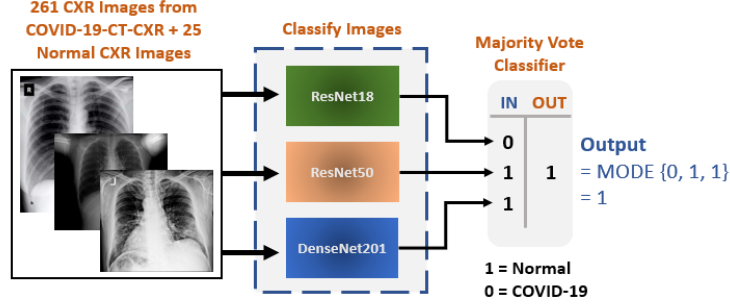


Figure 4: Bagging Approach [20] to Ensemble Learning using a Majority Vote Classifier

2.6 Experimental Setup

The transfer learning models were trained using the MATLAB programming language. CNN models (ResNet18, ResNet50, and DenseNet201) were pretrained on a subset of the ImageNet dataset which is used in the ImageNet Large-Scale Visual Recognition Challenge (ILSVRC) consisting of over a million images and a thousand class labels. For each network, the last three layers – fully connected, softmax, and classification layer – are replaced with the weights randomly initialized. Each network was trained for 15 epochs with a batch size and learning rate of 8 and 0.00005, respectively. As a cross-validation method, k-fold is chosen as a strategy to combat the limited data samples. The dataset split was 20% test set and 80% training set in each fold. K-fold cross-validation is used to ensure that each observation from the raw dataset can appear in both the training and testing set. Results were obtained using 5 different k values (1-5). Then each network is combined into a bagging ensemble neural network. This bagging ensemble uses a majority vote classifier which takes the mode of each output of the combined neural networks as seen in Figure 4. It is expected that a bagging ensemble will outperform any individual network model.

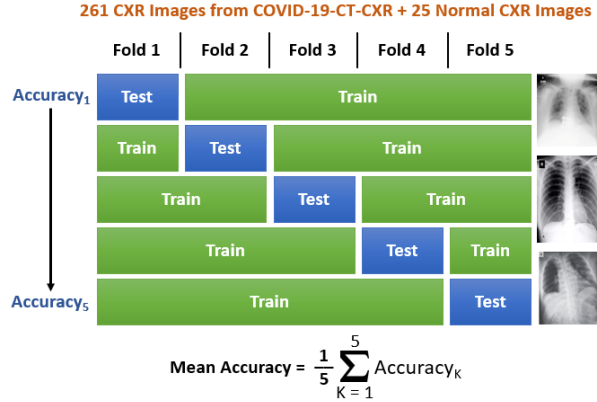


Figure 5: Visual Display of K-fold Cross-validation (k = 1-5)

2.7 Performance Metrics

TP, FP, TN, and FN given in Figure 6 represent True Positive, False Positive, True Negative, and False Negative percentages, respectively. Diagnostic testing necessitates a low False Negative (FN) rate or high sensitivity often at the risk of increasing the False Positive (FP) rate. These values are used in Equations (1) - (7) as evaluation metrics for the effectiveness of each neural network:

1. $Accuracy = \frac{(TN+FP)}{(TN+TP+FN+FP)}$
2. $Sensitivity = \frac{TP}{(TP+FN)}$
3. $Specificity = \frac{TN}{(TN+FP)}$
4. $Precision = \frac{TP}{(TP+FP)}$
5. $NegativePredictiveValue = \frac{TN}{(TN+FN)}$

$$6. F1Score = 2 \left[\frac{Precision * Recall}{Precision + Recall} \right]$$

$$7. FalsePositiveRate = \frac{FP}{(FP+TN)}$$

		Expected/Target Class		
		covid-Xray	normal	
Actual/Output Class	covid-Xray	TP True Positive	FP False Positive	Precision
	normal	FN False Negative	TN True Negative	Negative Predictive Value
		Sensitivity	Specificity	Accuracy

Figure 6: Confusion Matrix for Applied Deep Learning

Free-response receiver operating characteristic (FROC) curves allows for the evaluation of neural network performance at all classification thresholds. A classification threshold is the neural network’s resistance against labeling an image as positive (COVID-19); further expounding, the decision threshold is a neural network’s likelihood of classifying an image as negative (Normal). For medical diagnostic purposes, it is imperative that all positive cases are correctly classified. Therefore, a lower decision threshold is preferred. At each decision threshold, the sensitivity or true positive rate (TPR) as found in Equation (2) is plotted in the y-axis against the ‘average FPs per image’ or false positive rate (FPR) as found in Equation (7). As the threshold is lowered, both the TPR and FPR increase or remain constant. Area under the ROC curve (AUC) aggregates the performance of the neural network on all decision thresholds. This represents an average performance for the neural network. The closer the AUC is to 1.0, the better the network is at distinguishing between positive and negative classes.

3 Results and Discussion

In this study, ResNet18, ResNet50, and DenseNet201 have been trained on chest X-ray images from the COVID-19-CT-CXR dataset. Each network has a confusion matrix, FROC curve, and their 95% confidence intervals demonstrating their performance on several metrics. ResNet18 achieved the highest precision (99.6%) of each of the trained networks while ResNet50 achieved the highest sensitivity (99.6%) of each of the trained networks. The two networks were combined in a bagging ensemble alongside DenseNet201 to achieve a network with both a high precision and sensitivity of 99.6% and 100%, respectively. Our evaluation also shows that the bagging ensemble method achieves the best performance for classification (overall accuracy: 99.7%, 95% confidence interval: 87.75%–94.22%). The lowest performance values were yielded by DenseNet201 with a sensitivity and negative predictive value of 98.5% and 85.2%, respectively. Across the three neural networks, only one CXR images was a false positive between two of them, and no CXR images were false negatives implying that ResNet18 and DenseNet201 tend to identify disparate features in labeling false negatives – a desirable characteristic.

3.1 Figures and Tables

Neural Network	TP	FP	TN	FN	Accuracy	AUC	Confidence Interval (95%)
ResNet18	90.2%	0.3%	8.4%	1%	98.6%	0.99908	84.69 – 91.82
ResNet50	90.9%	0.7%	8.0%	0.3%	99.0%	0.98751	86.53 – 93.12
DenseNet201	89.9%	0.7%	8.0%	1.5%	97.9%	0.98958	86.98 – 93.69
Ensemble NN	91.3%	0.3%	8.4%	0%	99.7%	0.99954	87.75 – 94.22

Table 2: Confusion Matrix Values of Each Neural Network (k = 1-5)

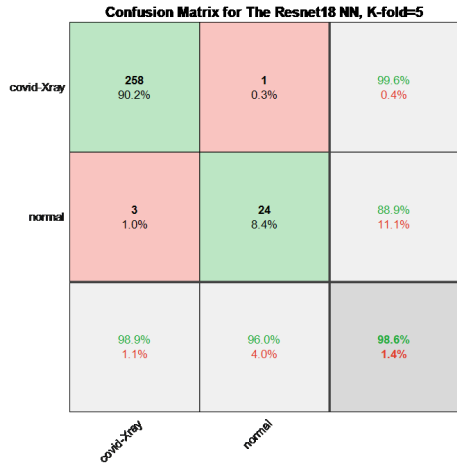


Figure 7: Confusion Matrix for ResNet18

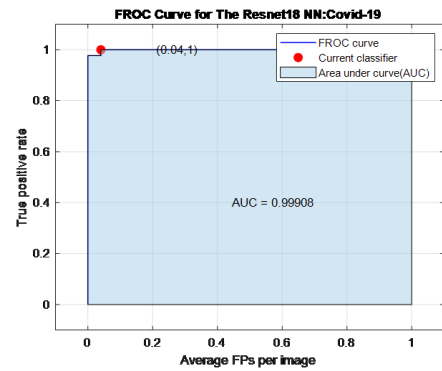


Figure 8: FROC Curve for ResNet18

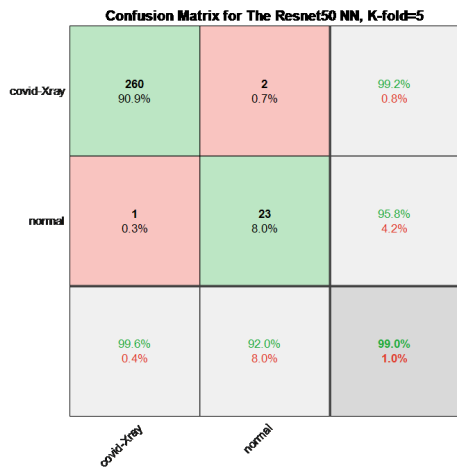


Figure 9: Confusion Matrix for ResNet50

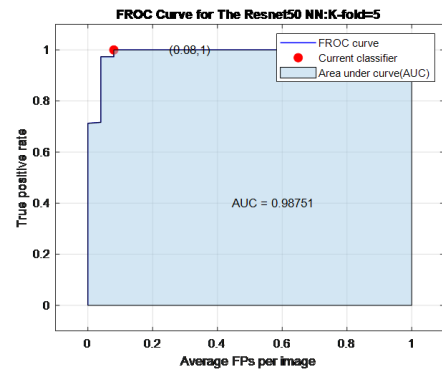


Figure 10: FROC Curve for ResNet50

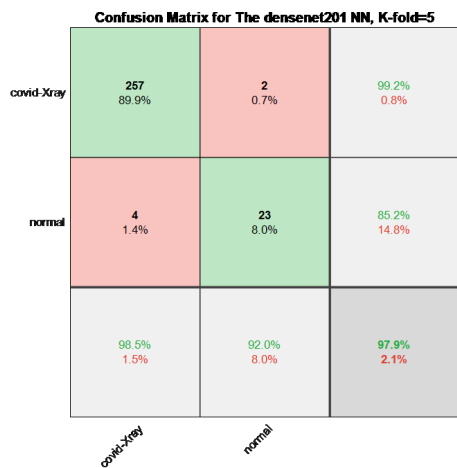


Figure 11: Confusion Matrix for DenseNet201

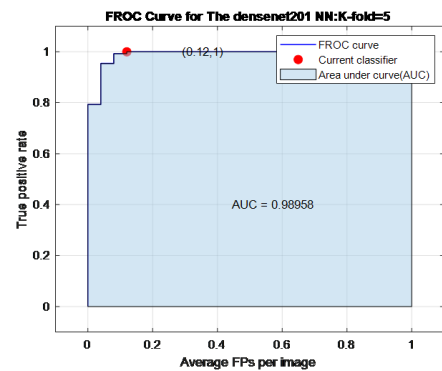


Figure 12: FROC Curve for DenseNet201

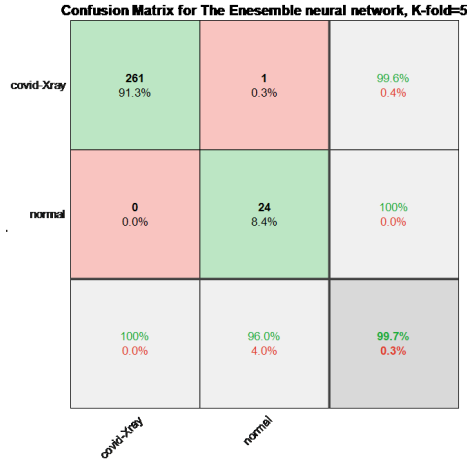


Figure 13: Confusion Matrix for Ensemble Neural Network

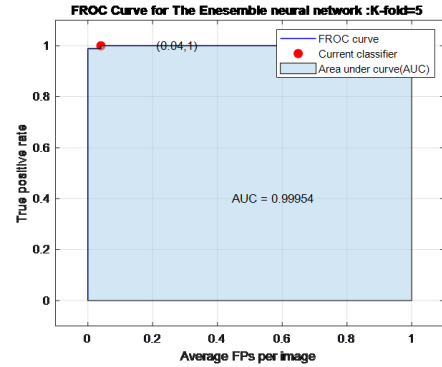


Figure 14: FROC Curve for Ensemble Neural Network

4 Conclusion

Early, relatively inexpensive, and sanitary detection of COVID-19 is of utmost importance during the current stages of the Coronavirus pandemic. By training deep transfer learning models and combining their outputs into a majority vote ensemble, we propose an effective binary classifier for CXR imagery as a first-line triage tool for hospitals and radiology services worldwide. Through ResNet50’s exceptional performance alongside ResNet18 and DenseNet201’s complementary image detection characteristics, an ensemble neural network with only one mislabeled CXR image of amongst a total of 286 CXR images is achieved. This study gives insight into how ensemble neural network architectures can be used to increase performance, and it is believed that this work can contribute to lessening the burden on radiology services. Further research can be performed by experimenting with new convolutional neural network architectures or with different ensemble techniques such as the boosting approach; additionally, there is potential to extend this work beyond a binary classifier into nuanced multi-outputs (viral pneumonia, inflammatory diseases, etc.).

References

- [1] Ho Yuen Frank Wong, Hiu Yin Sonia Lam, Ambrose Ho-Tung Fong, Siu Ting Leung, Thomas Wing-Yan Chin, Christine Shing Yen Lo, Macy Mei-Sze Lui, Jonan Chun Yin Lee, Keith Wan-Hang Chiu, Tom Chung, et al. Frequency and distribution of chest radiographic findings in covid-19 positive patients. *Radiology*, page 201160, 2020.
- [2] Linda Wang and Alexander Wong. Covid-net: A tailored deep convolutional neural network design for detection of covid-19 cases from chest x-ray images. *arXiv preprint arXiv:2003.09871*, 2020.
- [3] Adam Jacobi, Michael Chung, Adam Bernheim, and Corey Eber. Portable chest x-ray in coronavirus disease-19 (covid-19): A pictorial review. *Clinical Imaging*, 2020.
- [4] Michael Chung, Adam Bernheim, Xueyan Mei, Ning Zhang, Mingqian Huang, Xianjun Zeng, Jiufa Cui, Wenjian Xu, Yang Yang, Zahi A Fayad, et al. Ct imaging features of 2019 novel coronavirus (2019-ncov). *Radiology*, 295(1):202–207, 2020.
- [5] Ming-Yen Ng, Elaine YP Lee, Jin Yang, Fangfang Yang, Xia Li, Hongxia Wang, Macy Mei-sze Lui, Christine Shing-Yen Lo, Barry Leung, Pek-Lan Khong, et al. Imaging profile of the covid-19 infection: radiologic findings and literature review. *Radiology: Cardiothoracic Imaging*, 2(1):e200034, 2020.
- [6] Shuchang Zhou, Yujin Wang, Tingting Zhu, and Liming Xia. Ct features of coronavirus disease 2019 (covid-19) pneumonia in 62 patients in wuhan, china. *American Journal of Roentgenology*, 214(6):1287–1294, 2020.
- [7] Adam Bernheim, Xueyan Mei, Mingqian Huang, Yang Yang, Zahi A Fayad, Ning Zhang, Kaiyue Diao, Bin Lin, Xiqi Zhu, Kunwei Li, et al. Chest ct findings in coronavirus disease-19 (covid-19): relationship to duration of infection. *Radiology*, page 200463, 2020.

- [8] Redha Ali and Hussin K Ragb. Fused deep convolutional neural networks based on voting approach for efficient object classification. In *2019 IEEE National Aerospace and Electronics Conference (NAECON)*, pages 335–339. IEEE, 2019.
- [9] Yifan Peng, Yu-Xing Tang, Sungwon Lee, Yingying Zhu, Ronald M Summers, and Zhiyong Lu. Covid-19-ct-cxr: a freely accessible and weakly labeled chest x-ray and ct image collection on covid-19 from biomedical literature. *arXiv preprint arXiv:2006.06177*, 2020.
- [10] Satoshi Tsutsui and David J Crandall. A data driven approach for compound figure separation using convolutional neural networks. In *2017 14th IAPR International Conference on Document Analysis and Recognition (ICDAR)*, volume 1, pages 533–540. IEEE, 2017.
- [11] Sergey Zagoruyko and Nikos Komodakis. Wide residual networks. *arXiv preprint arXiv:1605.07146*, 2016.
- [12] Gao Huang, Zhuang Liu, Laurens Van Der Maaten, and Kilian Q Weinberger. Densely connected convolutional networks. In *Proceedings of the IEEE conference on computer vision and pattern recognition*, pages 4700–4708, 2017.
- [13] Yoshua Bengio, Patrice Simard, and Paolo Frasconi. Learning long-term dependencies with gradient descent is difficult. *IEEE transactions on neural networks*, 5(2):157–166, 1994.
- [14] Geoffrey E Hinton, Nitish Srivastava, Alex Krizhevsky, Ilya Sutskever, and Ruslan R Salakhutdinov. Improving neural networks by preventing co-adaptation of feature detectors. *arXiv preprint arXiv:1207.0580*, 2012.
- [15] Hussin K Ragb and Vijayan K Asari. Histogram of oriented phase (hop): a new descriptor based on phase congruency. In *Mobile Multimedia/Image Processing, Security, and Applications 2016*, volume 9869, page 98690V. International Society for Optics and Photonics, 2016.
- [16] Chuanqi Tan, Fuchun Sun, Tao Kong, Wenchang Zhang, Chao Yang, and Chunfang Liu. A survey on deep transfer learning. In *International conference on artificial neural networks*, pages 270–279. Springer, 2018.
- [17] Jason Yosinski, Jeff Clune, Yoshua Bengio, and Hod Lipson. How transferable are features in deep neural networks? In *Advances in neural information processing systems*, pages 3320–3328, 2014.
- [18] Redha Ali, Russell C Hardie, Barath Narayanan Narayanan, and Supun De Silva. Deep learning ensemble methods for skin lesion analysis towards melanoma detection. In *2019 IEEE National Aerospace and Electronics Conference (NAECON)*, pages 311–316. IEEE, 2019.
- [19] Barath Narayanan Narayanan, Redha Ali, and Russell C Hardie. Performance analysis of machine learning and deep learning architectures for malaria detection on cell images. In *Applications of Machine Learning*, volume 11139, page 111390W. International Society for Optics and Photonics, 2019.
- [20] Richard Maclin and David Opitz. Popular ensemble methods: An empirical study. *arXiv*, pages arXiv–1106, 2011.